TE Modes of an Axially Multiple-Grooved Rectangular Waveguide

Kurt P. Ericksen, *Member, IEEE*, and Altan M. Ferendeci, *Member, IEEE*

Abstract— **A method is developed to calculate the TE mode fields and cut-off frequencies of an axially multiple-grooved rectangular (AGR) waveguide. A low frequency AGR waveguide is used as a part of a microwave cavity and the cut-off frequencies are measured in order to verify the analytically derived results. Excellent agreement between the measured and calculated values provide the basis for the design of waveguides for millimeter wave applications. The method has also been extended to a waveguide with multiple grooves cut into two of its broad wall parallel surfaces.**

I. Introduction

THIS PAPER presents a method for finding the TE modes of an axially grooved rectangular (AGR) waveguide. As shown in Fig. 1, a waveguide of this type has N uniformly spaced axial grooves cut into one of the broad surfaces. A particular application for this type of waveguide is a cavity for the interaction region of a high harmonic rectangular gyrotron [1].

The output frequency of a gyrotron is directly proportional to the axial magnetic field [2]. Operation of the gyrotron at millimeter wavelengths require superconducting magnets. Since gyrotrons are quasi-relativistic devices, harmonic operation has also high efficiency [3]. Using higher harmonics one can utilize lower magnetic fields which are within the confines of conventional electromagnets. It has been proposed that by using an axis encircling pencil beam in an axially grooved magnetron type cylindrical geometry, the high harmonic operation of the gyrotron is highly enhanced [4]. As the current density increases, the space charge effects in the pencil beam become dominant, leading to large velocity spread, thus making the operation at the higher power levels limited. Replacing the axially grooved cylindrical geometry and the pencil beam by an axially grooved rectangular waveguide and a rotating ribbon beam, some of these problems can be reduced [5]. The grooves enhance the interaction between the electrons and the fields, and at the same time reduce the number of competing modes. The mode excitation is controlled by the dimensions of the axial grooves. Use of the ribbon beam also allows the spread of the same current over a larger cross sectional area, thus reducing the space charge effects.

When used in this manner, a quasi-relativistic sheet electron beam injected into the AGR cavity interacts with the cavity electromagnetic fields. The geometry can be thought of as the convolution of the rising-sun type axially grooved cylindrical waveguides used in magnetrons [6]. Since the optimum interaction always occurs with the TE modes of the cavity and the interaction with TM modes is insignificant with regards to the gyrotron applications, only the calculations and experimental verification of the cut-off frequencies of the TE modes for the AGR waveguide are presented. The type of waveguide presented here is completely different than the usual slow wave periodic structures which contain grooves transverse to the direction of propagation.

The waveguide shown in Fig. 1 is made up of two regions. Region I consists of the main body of the waveguide and Region II is made up of N uniform axial grooves cut into one of the broad surfaces (singly-grooved) of the waveguide. In order to find the cut-off frequencies, solutions to the Helmholtz equation which satisfy the proper boundary conditions have been found in the two regions. Although the analytical results can be derived in a closed form, only a numerical solution of the dispersion equation is possible as a result of the complicated geometry. As expected, solution for the waveguide problem occurs only for the discrete values of cut-off wavenumbers. These are then used in a cavity configuration to verify experimentally the resulting TE cut-off frequencies for the waveguide.

In Section II, the solutions to the Helmholtz equation and the derivation of the corresponding fields and the resulting dispersion relation are given. In Section III, the numerical solution for the cut-off frequencies of various TE modes as well as the electric field plots are presented. The solution is extended to the doubly-grooved (grooved on both broad surfaces) AGR waveguide. Section IV includes an experimental verification of the cut-off frequencies of the AGR waveguide by using the resonant modes of a test cavity made from the given waveguide.

II. Field Expression and the Dispersion Equation

In Fig. 1, a is the x-dimension and b is the y-dimension of the uniform section of the waveguide. $2L$ is the unit cell length, $2W$ is the groove width, and d is the groove depth. The last three dimensions are assumed to be identical for each unit cell. There are N grooves (N unit cells). The length L is found from $L = a/2N$. Although for the general waveguide problem, there are no restrictions on the waveguide cross sectional dimensions, application to a AGR gyrotron imposes restrictions on some of these waveguide dimensions. For example, in this case, b should be greater than $2R_L$, where

Manuscript received August 10, 1992; revised May 25, 1995. This work is supported in part by Air Force Office of Scientific Research.

The authors are with the Electrical and Computer Engineering and Computer Science Department, University of Cincinnati, Cincinnati, OH 45221 USA.

IEEE Log Number 9413421.

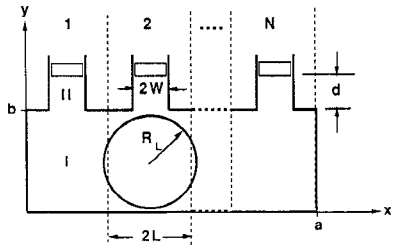

Fig. 1. Transverse cross section of the AGR waveguide.

R_L is the Larmor radius of the electrons and a should be slightly greater than the width of the interacting sheet beam.

Solution of the Helmholtz equation $\nabla^2 H_z + k^2 H_z = 0$ is found for the two regions separately. In region II, fields that satisfy the necessary boundary conditions are of the form [5]

$$E_x = E_o \frac{\sin[k_{co}(d+b-y)]}{\sin(k_{co}d)} \cos\left[\frac{i(2q-1)\pi}{2N}\right] \quad (1)$$

$$E_y = 0 \quad (2)$$

$$H_z = \frac{jk_{co}E_o}{\omega\mu} \frac{\cos[k_{co}(d+b-y)]}{\sin(k_{co}d)} \cos\left[\frac{i(2q-1)\pi}{2N}\right] \quad (3)$$

where k_{co} is the equivalent rectangular waveguide cut-off wave number, q is the groove number, and i is an integer that determines the phase difference between the grooves. The term i is defined by

$$\Psi = \frac{i\pi}{N}. \quad (4)$$

Here $i = 0, \cdots, N-1$ and Ψ is the phase difference between successive grooves. For $i = 0, \Psi = 0$, the electric field has the same magnitude and phase at the entrance to every groove. Also, the value for E_x at the groove entrance is a maximum. This results in maximum electron beam interaction when the waveguide is the interaction region of a high harmonic rectangular gyrotron. This case is referred to as the 2π mode and the AGR cavity is designed so that it supports this mode. The other modes are designated by their effect on Ψ with the appropriate values for i and N substituted into (4). For example, with $i = 1, N = 3$, (4) gives $\Psi = \pi/3$, which is referred to as the $\pi/3$ mode [7].

For $y = b$, (1) gives a constant electric field across the groove entrance. This is an approximation to the actual electric field. A more accurate assumption for the fields, which takes into account the fringing fields at the entrance to the groove, is given in the Appendix. However, it is shown in the Appendix that if the groove depth to groove pitch ratio $d/2L$ is small, the constant field approximation still gives very accurate results.

Next, it is necessary to find the field expressions in Region I. For a waveguide in cutoff, the transverse components of the magnetic field are zero. Therefore, the TE field components in Region I are E_x, E_y, and H_z. The field expressions in the AGR waveguide have the same form as those found for a rectangular waveguide. The infinite sum formulation for the three field components are [8]

$$E_x = \sum_{n=-\infty}^{\infty} \frac{j\omega\mu k_{yn}}{k_{co}^2} C_n \cos(k_{xn}x)\sin(k_{yn}y) \quad (5)$$

$$E_y = \sum_{n=-\infty}^{\infty} \frac{-j\omega\mu k_{xn}}{k_{co}^2} C_n \sin(k_{xn}x)\cos(k_{yn}y) \quad (6)$$

$$H_z = \sum_{n=-\infty}^{\infty} C_n \cos(k_{kn}x)\sin(k_{yn}y) \quad (7)$$

where

$$k_{xn} = \frac{n\pi}{a} \quad (8)$$

$$k_{yn}^2 = k_{co}^2 - k_{xn}^2. \quad (9)$$

To determine the expansion coefficients C_n in (5)–(7), the boundary condition which requires the electric fields of the two regions to be equal at the groove entrance is used. Substituting $y = b$ into (1) and (5), and multiplying both sides by $\cos(k_{xm}x) = \cos(m\pi x/a)$ and integrating from 0 to a results in

$$C_n = \begin{cases} \dfrac{k_{co}^2 E_o}{j\omega\mu k_{yn}} \dfrac{(-1)^m N \sin\left(\dfrac{n\pi W}{a}\right)}{n\pi \sin(k_{yn}b)} & \text{if } n = 2mN \pm i \\ 0 & \text{otherwise} \end{cases} \quad (10)$$

where m is an integer.

Substituting (10) into (5)–(7) gives the expressions for the fields in the main body of the AGR waveguide. These are

$$E_x = E_o \sum_{m=-\infty}^{\infty} (-1)^m N \cdot \left\{ \frac{\sin(k_{xn^+}W)}{n^+\pi} \cos(k_{kn^+}y) \frac{\sin(k_{yn^+}y)}{\sin(k_{yn^+}b)} + \frac{\sin(k_{xn^-}W)}{n^-\pi} \cos(k_{xn^-}x) \frac{\sin(k_{yn^-}y)}{\sin(k_{yn^-}b)} \right\} \quad (11)$$

$$E_y = E_o \sum_{m=-\infty}^{\infty} (-1)^{m+1} N \cdot \left\{ \frac{k_{xn^+}}{n^+\pi} \sin(k_{xn^+}W)\sin(k_{xn^+}x) \frac{\cos(k_{yn^+}y)}{k_{yn^+}\sin(k_{yn^+}b)} + \frac{k_{xn^-}}{n^-\pi} \sin(k_{xn^-}W)\sin(k_{xn^-}x) \frac{\cos(k_{yn^-}y)}{k_{yn^-}\sin(k_{yn^-}b)} \right\} \quad (12)$$

$$H_z = \frac{k_{co}^2 E_o}{j\omega\mu} \sum_{m=-\infty}^{\infty} (-1)^m N \cdot \left\{ \frac{\sin(k_{xn^+}W)}{n^+\pi} \cos(k_{kn^+}x) \frac{\cos(k_{yn^+}y)}{k_{yn^+}\sin(k_{yn^+}b)} + \frac{\sin(k_{xn^-}W)}{n^-\pi} \cos(k_{xn^-}x) \frac{\cos(k_{yn^-}y)}{k_{yn^-}\sin(k_{yn^-}b)} \right\} \quad (13)$$

where

$$n^+ = 2mN + i, \quad k_{kn^+} = \frac{n^+\pi}{a}, \quad k_{yn^+}^2 = k_{co}^2 - k_{xn^+}^2$$

$$n^- = 2mN - i, \quad k_{xn^-} = \frac{n^-\pi}{a}, \quad k_{yn^-}^2 = k_{co}^2 - k_{xn^-}^2. \quad (14)$$

The amplitude E_o is determined from the input power supplied to the waveguide.

The wave number k_{co} is found by matching the average magnetic field in region I to the magnetic field in region II at the entrance to each groove [5]. The average magnetic field in region I is found from

$$\tilde{H} = \frac{1}{2W}\int_{((2q-1)a/2N)-W}^{((2q-1)a/2N)+W} H_x(y=b)\,dx = \frac{E_o W k_{co}}{j2\omega\mu L}\cos\left[\frac{i(2q-1)\pi}{2N}\right] \cdot \left\{\sum_{m=-\infty}^{\infty}(-1)^m \frac{\sin^2\left(\frac{n^+\pi W}{a}\right)}{\left(\frac{n^+\pi W}{a}\right)^2}\frac{\cot(k_{yn^+}b)}{k_{yn^+}} + \sum_{m=-\infty}^{\infty}(-1)^m \frac{\sin^2\left(\frac{n^-\pi W}{a}\right)}{\left(\frac{n^-\pi W}{a}\right)^2}\frac{\cot(k_{yn^-}b)}{k_{yn^-}}\right\}. \quad (15)$$

The magnetic field for region II at the groove entrance is found by substituting $y = b$ into (3). Equating these two expressions gives the dispersion equation for the AGR waveguide

$$-\frac{\cot(k_{co}d)}{k_{co}} = \frac{W}{2L}\sum_{m=-\infty}^{\infty}(-1)^m \frac{\sin^2\left(\frac{n^+\pi W}{a}\right)}{\left(\frac{n^+\pi W}{a}\right)^2}\frac{\cot(k_{yn^+}b)}{k_{yn^+}} + \frac{W}{2L}\sum_{m=-\infty}^{\infty}(-1)^m \frac{\sin^2\left(\frac{n^-\pi W}{a}\right)}{\left(\frac{n^-\pi W}{a}\right)^2} \cdot \frac{\cot(k_{yn^-}b)}{k_{yn^-}}. \quad (16)$$

III. Cut-Off Frequencies

In order to complete the derivation of the AGR waveguide fields, the waveguide cutoff wave numbers, k_{co}, are to be determined. This is done by solving (16). The simplest way is to plot both the right and left hand sides of (16) on the same graph as a function of frequency. The intersection points of the two curves give the cut-off frequencies for that mode. The approximate result for the frequency from the plot is used as a starting condition for a more accurate numerical solution using the bisection method [9]. The corresponding modes are labeled as TE_{ik} modes where k stands for the kth cut-off frequency associated with the ith mode.

The AGR waveguide dimensions used when plotting (16) are given in Table I. The dispersion equation plots are shown in Fig. 2 for $i = 0(\Psi = 2\pi), i = 1(\Psi = \pi/3)$, and $i = 2(\Psi = 2\pi/3)$ modes up to 15 GHz. The cut-off frequencies f_{co} are found from k_{co} by

$$f_{co} = \frac{c}{2\pi}k_{co} \quad (17)$$

where c is the speed of light.

TABLE I
Test AGR Waveguide Dimensions

N	a	b	W	d
3	5.73 cm	2.71 cm	0.17 cm	0.84 cm

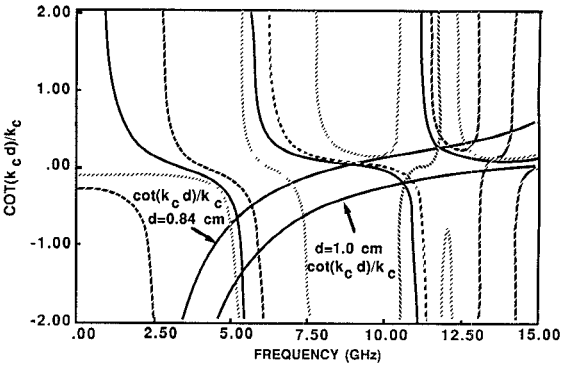

Fig. 2. The dispersion plots for AGR waveguide with grooves on one broad wall for $d = 0.84$ cm and $d = 1.0$ cm. (—) 2π ($i = 0$) mode, (- - -) $\pi/3$ ($i = 1$) mode, and ($\cdots$) $2\pi/3$ ($i = 2$) mode.

TABLE II
Cut-Off Frequencies for a Singly-Grooved and Doubly-Grooved Waveguide

mode	i	k	single f_{co} (GHz)	double f_{co} (GHz)
2π	0	1	5.1666	4.8941
		2	9.2994	10.526
		3	11.999	
$\pi/3$	1	1	2.5327	5.3786
		2	5.6927	10.841
		3	9.5519	13.611
$2\pi/3$	2	1	5.0165	6.5684
		2	7.0163	
		3	11.443	
		4	12.516	

Table II gives the calculated cut-off frequencies found from the numerical solution of the dispersion (16) for the singly-grooved AGR waveguide for $N = 3$.

A second plot of $-\cot(k_c d)/k_c$ for a different groove height $d = 1.0$ cm is also shown in Fig. 2. Changing the groove height changes the cut-off frequencies of the waveguide when all the other physical dimensions are kept constant. If provisions are made so that simultaneously movable mechanical sliding shorts can be introduced into the grooves, the cut-off frequency of a given mode can be changed by varying the depth d of the grooves. This allows the resulting cavity for the rectangular gyrotron to be frequency tunable.

Once k_{co} for a given mode is found, the corresponding transverse electric fields for the waveguide are known. They are then used to graphically plot the transverse electric field lines for each mode [10]. The AGR waveguide is periodic in the transverse (x) direction with a unit cell of length $2L$ for the 2π mode. Therefore, the field distribution is symmetric over each of the unit cells for the 2π mode. Electric field

plots corresponding to the $k = 1$ and $k = 3$ modes of the 2π mode for a singly-grooved waveguide are shown in Fig. 3. It is apparent that the fringing fields in the vicinity of the grooves are high for the $i = 0, k = 3$ mode. Thus, for a high harmonic gyrotron operation, this mode is therefore preferred over the $i = 0, k = 1$ and $k = 2$ modes.

To verify that the presence of the grooves, in addition to increasing the interaction efficiency, reduces the number of competing modes associated with the TE modes of a standard oversized waveguide, a similar derivation is applied to a rectangular waveguide with identical axial grooves at the two wider walls. Assuming that the fields at the grooves satisfy the same boundary conditions as the singly-grooved waveguide results in the following expressions for the fields and dispersion equation. The field expressions are

$$E_x = E_o \sum_{m=-\infty}^{\infty} (-1)^m N \cdot \left\{ \frac{\sin(k_{xn^+}W)}{n^+\pi} \cos(k_{kn^+}x) \frac{\cos(k_{yn^+}y)}{\cos(k_{yn^+}b/2)} + \frac{\sin(k_{xn^-}W)}{n^-\pi} \cos(k_{xn^-}x) \frac{\cos(k_{yn^-}y)}{\cos(k_{yn^-}b/2)} \right\} \quad (18)$$

$$E_y = E_o \sum_{m=-\infty}^{\infty} (-1)^{m+1} N \cdot \left\{ \frac{k_{xn^+}}{n^+\pi} \sin(k_{xn^+}W) \sin(k_{kn^+}x) \cdot \frac{\sin(k_{yn^+}y)}{k_{yn^+}\cos(k_{yn^+}b/2)} + \frac{k_{xn^-}}{n^-\pi} \sin(k_{xn^-}W) \sin(k_{xn^-}x) \cdot \frac{\sin(k_{yn^-}y)}{k_{yn^-}\cos(k_{yn^-}b/2)} \right\} \quad (19)$$

$$H_x = \frac{k_{co}^2 E_0}{j\omega\mu} \sum_{m=-\infty}^{\infty} (-1)^{m+1} N \cdot \left(\frac{\sin(k_{xn^+}w)}{n^+\pi} \cos(k_{kn^+}x) \frac{\sin(k_{yn^+}y)}{k_{yn^+}\cos(k_{yn^+}b/2)} + \frac{\sin(k_{xn^-}W)}{n^-\pi} \cos(k_{xn^-}x) \frac{\sin(k_{yn^-}y)}{k_{yn^-}\cos(k_{yn^-}b/2)} \right). \quad (20)$$

The dispersion equation is

$$-\frac{\cot(k_{co}d)}{k_{co}} = \frac{N}{W\pi} \sum_{m=-\infty}^{\infty} (-1)^{m+1} \cdot \frac{\sin^2(k_{xn^+}W)}{n^+k_{xn^+}} \frac{\tan(k_{yn^+}b/2)}{k_{yn^+}} \cdot + \frac{N}{W\pi} \sum_{m=-\infty}^{\infty} (-1)^{m+1} \cdot \frac{\sin^2(k_{xn^-}W)}{n^-k_{xn^-}} \frac{\tan(k_{yn^-}b/2)}{k_{yn^-}}. \quad (21)$$

Plot of (21) is given in Fig. 4. The dimensions and the number of grooves on both walls are the same as those given

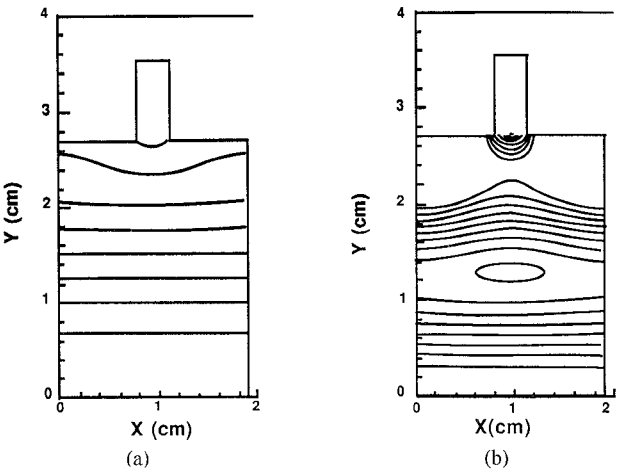

Fig. 3. Transverse electric field lines for the singly-grooved AGR waveguide 2π modes: a) $i = 0, k = 1$ mode, $f_{co} = 5.1666$ GHz, and b) $i = 0, k = 3$ mode, $f_{co} = 11.999$ GHz.

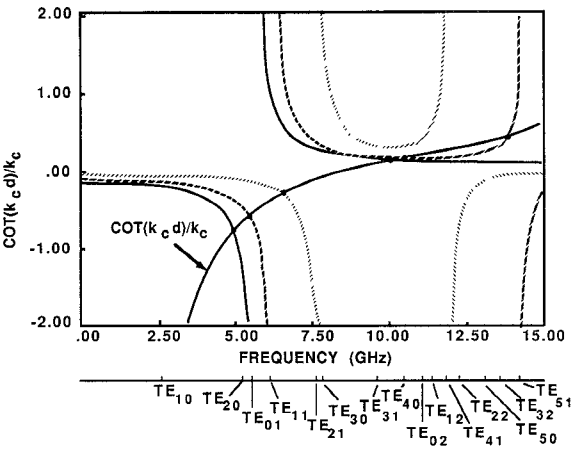

Fig. 4. The dispersion plots for AGR waveguide with grooves on both broad walls for $d = 0.84$ cm. (—) 2π ($i = 0$) mode, (- - - -) $\pi/3$ ($i = 1$) mode, and ($\cdots$) $2\pi/3$ ($i = 2$) mode. TE_{mn} modes of a grooveless rectangular waveguide are also plotted below the frequency scale.

for the singly-grooved waveguide. In Fig. 4, corresponding TE_{mn} cut-off frequencies for a grooveless waveguide with the same a and b dimensions are also shown below the frequency axis to compare the cut-off frequencies of the waveguide with and without grooves.

The calculated cut-off frequencies for a doubly-grooved AGR waveguide are also listed in Table II. The corresponding electric field distribution for the $k = 1$ and $k = 3$ modes of the 2π mode for a doubly-grooved waveguide with all the same dimensions given in Table I, except with $b = 5.15$ cm is plotted in Fig. 5.

IV. Experimental Verification of Cut-Off Modes

The theoretically calculated cut-off frequencies for the AGR waveguide are verified experimentally using a test cavity. A short length of the AGR waveguide ($D = 6.03$ cm) is machined with the transverse dimensions given in Table I. Two shorting plates are placed at each end. A small probe is inserted into the cavity through one of the side walls to excite the cavity as shown in Fig. 6.

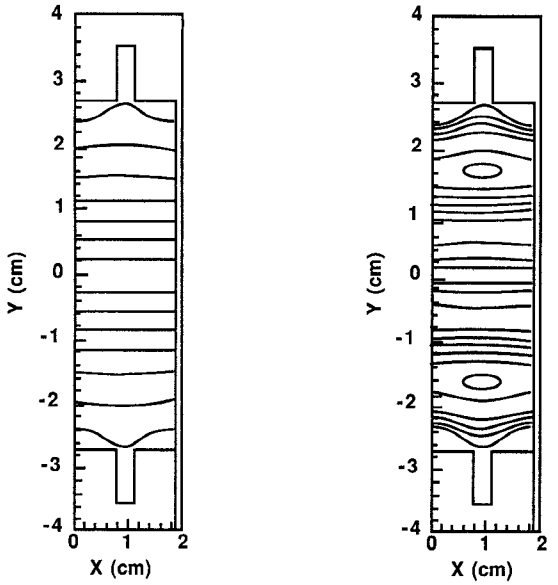

Fig. 5. Transverse electric field lines for the doubly-grooved AGR waveguide 2π modes ($b = 5.15$ cm): a) $i = 0, k = 1$ mode, $f_{co} = 2.6233$ GHz, and b) $i = 0. k = 3$ mode, $f_{co} = 13.633$ GHz.

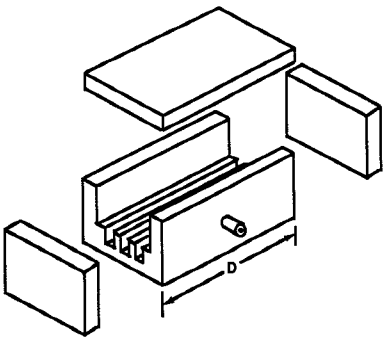

Fig. 6. AGR cavity for measuring resonant frequencies.

As a result of the shorting plates placed at the two ends of the waveguide, an axial standing wave is generated between these two planes. The resulting cavity resonance frequencies are given by

$$f_{c,ikl} = \frac{1}{2\pi\sqrt{\mu_o\varepsilon_o}}\left[(k_{co})_{ik}^2 + \left(\frac{l\pi}{D}\right)^2\right]^{1/2}. \qquad (22)$$

Here l is an integer and D is the length of the cavity in the z direction. The corresponding modes can be identified as TE_{ikl} resonant modes for the cavity. Here $(k_{co})_{ik}$ corresponds to the cut-off wave number of the AGR waveguide for the kth zero of the ith mode.

The TE_{ikl} cavity resonant frequencies are calculated from (22) up to 15 GHz using the previously calculated cut-off wave number k_{co} values given in Table II. These are tabulated in Table III. An HP-8510 microwave network analyzer is swept in frequency and the resonant frequencies of the test cavity are recorded. These frequencies are compared with the theoretically calculated results. Although there were additional resonances attributed to other modes such as TM modes, no attempt was made to identify these resonances. The measured resonant frequencies of the cavity which are close to the predicted resonant frequencies are also included in Table III.

TABLE III
CALCULATED AND MEASURED TE_{ik} RESONANT FREQUENCIES FOR THE TEST CAVITY

mode	i	k	l	$(f_c)_{ik}$	theoretical $(f_c)_{ikl}$	measured $(f_c)_{ikl}$
2π	0	1	1	9.2994	9.6264	9.6225
			3		11.924	11.985
$\pi/3$	1	1	1	2.5327	3.5502	3.5525
			3		7.8817	7.87
			5		12.695	12.678
		3	1	9.5519	9.8706	9.8875
			2		10.770	10.84
			3		12.122	12.13

V. DISCUSSION AND CONCLUSION

A comparison of the calculated resonant frequencies to the measured frequencies given in Table III shows excellent agreement. The greatest percent difference between calculated and measured results was 0.9%. The average percent difference for the test cavity was only 0.2%. Considering the constant field approximation at the groove opening, the measured frequencies are in close agreement.

Both of the dispersion relations given by (21) and (27) reduce to the cut-off wave numbers for a grooveless rectangular waveguide as d and W approach 0. As d approaches 0, the left side of both equations approach ∞. These are satisfied if both k_{yn+} and k_{yn-} are equal to $m\pi/b$ on the right side, This leads to the usual waveguide cut-off wave numbers $k_{co}^2 = (n\pi/a)^2 + (m\pi/b)^2$.

When the number of grooves is equal to one, axially grooved waveguide presented here is equivalent to a channel waveguide [11]. For a channel waveguide, the cut-off frequency f_c is calculated and compared with the cut-off frequency $f_{c|\mathrm{TE}10}$ of the TE_{10} mode of a grooveless rectangular waveguide with the same a and b dimensions. For the following parameters $b/a = 0.455$, $(d + b)/b = 0.5$, and $W/L = 0.23$ with $a = 1.91$ cm, the ratio $f_{c|\mathrm{TE}10}/f_c$ is equal to 1.09 for the channel waveguide [11]. Using the same parameters, (16) is plotted for $N = 1$ and the resulting lowest order mode cut-off frequency f_c of the AGR is calculated. For this case, the ratio of $f_{c|\mathrm{TE}10}/f_c$ is found to be 1.07. Thus, the calculations presented here also agree with the results of the channel waveguide.

As can be seen from Table II, if the same number of axial grooves are introduced on the second broad-surface of the waveguide, the number of TE modes supported by the waveguide decreases, thus further reducing the mode competition problems associated with oversized waveguides.

Extending the calculation presented here to millimeter wavelengths is straight forward. For example, if operation at 90 GHz and sixth harmonic is desired, the Larmor radius for the fundamental cyclotron frequency of 15 GHz is calculated for a given beam energy. The dimension b is chosen slightly

larger that $2R_L$. Once the width of the rotating sheet beam is given, the overall dimension a and the number of grooves N can be chosen. By using (16) and by a repeated numerical calculation process, the groove width W and the groove depth d can then be determined to provide the desired cut-off frequency of the TE_{ok} mode at 90 GHz for the 2π mode ($i = 0$). Since various combinations of W and d will satisfy this condition, it is very important that the cut-off frequencies of the other TE_{oj} modes ($j = 1 \cdots k-1$) of the grooved waveguide do not coincide with any of the lower harmonics of the fundamental cyclotron frequency to prevent oscillations at lower frequencies.

The close agreement between the experimentally measured cut-off frequencies with the theoretically predicted values as well as the behavior of the field lines at the boundaries of the waveguide provide a proof to the validity of the assumptions made with regards to these calculations.

APPENDIX

A common practice for finding the solutions at a waveguide discontinuity is to assume a solution at the discontinuity. In this paper, a constant field at the entrance of the grooves is assumed. However, a more accurate assumed solution is the quasi-static gap field also referred to as the electrostatic fringe field [4], [6], [7].

Assuming this type of field at the entrance to the groove changes the constant term E_o of (1) and (3). There is now an x-dependence to the fields. This is given by [6]

$$E_o = \frac{P}{\sqrt{1-\left(\dfrac{x-(2q-1)L}{W}\right)^2}} \tag{23}$$

where P is a constant. The fields in region II are now of the form

$$E_x = \frac{P}{\sqrt{1-\left(\dfrac{x-(2q-1)L}{W}\right)^2}} \frac{\sin\left[k_{co}(d+b-y)\right]}{\sin\left(k_{co}d\right)} \cdot \cos\left[\frac{i(2q-1)\pi}{2N}\right] \tag{24}$$

$$E_y = 0 \tag{25}$$

$$H_x = \frac{P}{\sqrt{1-\left(\dfrac{x-(2q-1)L}{W}\right)^2}} \frac{jk_{co}}{\omega\mu} \frac{\cos\left[k_{co}(d+b-y)\right]}{\sin\left(k_{co}d\right)} \cdot \cos\left[\frac{i(2q-1)\pi}{2N}\right]. \tag{26}$$

Equation (26) is used to find the new expansion coefficient C_n for (5)–(7). The new resonant condition is found using the same procedure given in Sections III and IV. The resulting resonance condition for the fringing field assumption is

$$-\frac{\cot\left(k_{co}d\right)}{k_{co}} = \sum_{m=-\infty}^{\infty} (-1)^m \frac{\sin\left(\dfrac{n^+\pi W}{a}\right)}{n^+\pi} \cdot J_o\left(\frac{n^+\pi W}{a}\right) \frac{\cot\left(k_{yn^+}b\right)}{k_{yn^+}} + \sum_{m=-\infty}^{\infty} (-1)^m \frac{\sin\left(\dfrac{n^-\pi W}{a}\right)}{n^-\pi} \cdot J_o\left(\frac{n^-\pi W}{a}\right) \frac{\cot\left(k_{yn^-}b\right)}{k_{yn^-}} \tag{27}$$

where J_o is the zeroth order Bessel Function of the first kind.

The difference in the resonant frequencies found from (16) and (25) is within 5% if the ratio $d/2L < 0.15$. The ratio $d/2L$ is groove width to groove pitch ratio.

REFERENCES

[1] A. M. Ferendeci, "Rectangular cavity high harmonic gyrotron amplifier," in *IEEE MTT-S Dig.*, Boston, MA, vol. N-9, May 1983, pp. 430–431.

[2] L. J. Craig, "Status of gyrotron development," *J. Fusion Energy*, vol. 6, pp. 351–360, 1987.

[3] K. R. Chu, "Theory of electron cyclotron maser interaction in a cavity at the harmonic-frequencies," *Phys. Fluids*, vol. 21, pp. 2354–2364, 1978.

[4] Y. Y. Lau and L. R. Barnett, " Theory of low magnetic field gyrotron (Gyromagnetron)," *Int. J. Infrared and Millimeter Waves*, vol. 3, p. 619, 1982.

[5] C. C. Han and A. M. Ferendeci, "Non-linear analysis of a high harmonic rectangular gyrotron," *Int. J. Electron.*, vol. 57, pp. 1055–1063, 1984.

[6] N. M. Kroll and W. E. Lamb, "The resonant modes of the rising sun and other unstrapped magnetron anode blocks," *J. Appl. Phys.*, vol. 19, no. 2, pp. 166–186, 1948.

[7] R. G. E. Hutter, *Beam and Wave Electronics in Microwave Tubes*, 1st ed. Princeton, NJ: D. Van Nostrand, 1960.

[8] H. Motz, *Electromagnetic Problems of Microwave Theory*, 1st ed., Methuen & Co,. Ltd., 1951.

[9] S. Chapra and R. P. Camale, *Introduction to Computing for Engineers*. New York: McGraw-Hill, 1986.

[10] P. E. Moller and R. H. Macphie, "On the graphical representation of electric fields in waveguide," *IEEE Trans. Microwave Theory Tech.*, vol. 33, pp. 187–192, 1985.

[11] R. J. Vilmur and K. Ishii, "The channel waveguide," *IRE Trans. Microwave Theory Tech.*, vol. 10, pp. 220–221, 1962.

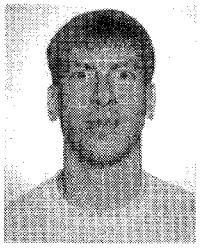

Kurt P. Ericksen (S'86–M'93) received the B.S. and Ph.D. degrees from the University of Cincinnati and M.S. degree from Ohio State University in 1985, 1988, and 1992, respectively. His graduate research was in the areas of semiconductor physics and applied electromagnetics. Particular focus was on high power millimeter wave tubes.

In 1993, he joined Motorola Paging Products Group, Schaumburg, Illinois, where he has worked on transmitter design for paging infrastructure applications.

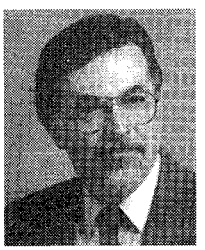

Altan M. Ferendeci (M'63) is a Faculty Member at the Electrical and Computer Engineering and Computer Science Department at the University of Cincinnati. He is also the director of the Millimeter Wave Electronics Laboratory. His interests are in microwaves and millimeter wave devices and circuits, microwave applications of high temperature superconductors, electro-optics, electron beam devices and gyrotrons. In addition to being author and co-author of various papers and conference proceedings, he is also the author of a text book *Physical Foundations of Solid State and Electron Devices* and co-editor of the book *Atomic and Molecular Processes in Controlled Thermonuclear Research.*